Theor Chem Acc (2012) 131:1163
DOI 10.1007/s00214-012-1163-5

REGULAR ARTICLE

Improved stability of water clusters $(H_2O)_{30–48}$: a Monte Carlo search coupled with DFT computations

Fengyu Li · Yuan Liu · Lu Wang · Jijun Zhao · Zhongfang Chen

Received: 9 October 2011 / Accepted: 11 November 2011 / Published online: 2 March 2012

Abstract The growing structural patterns of water clusters with 30–48 water molecules were investigated by means of a combined Monte Carlo search algorithm and density functional theory computations. The $(H_2O)_{30–48}$ clusters with amorphous core–shell structures are lower in energy than the previously reported fused cage and the tubular configurations. The significant differences in infrared spectra of these three different structural patterns provide some clues to identify the structural properties of these medium-sized water clusters in experiments.

Keywords Water clusters · Structures · Stabilization energy · Infrared spectrum

1 Introduction

As an eternal theme, water has been attracting scientists to reveal its mysterious veil both experimentally and theoretically [1]. For example, at some nanoscale, water does not freeze even below 0 °C, due to the distorted hydrogen bonds (H-bonds) [2–4]. Water transportation across biological and nanoscale channels and the wetting properties of the solid surfaces with nanoscale patterned structures were investigated by means of molecular dynamics (MD) simulation with empirical potentials [5–8]. More interestingly, MD simulations by Hamm and coworkers revealed that water molecules in bulk actually form two different microscopic constructions that break apart and recombine on the order of 200–400 fs [9]. All these findings evidenced the complicity of water, as H. E. Stanley said "*We will never understand biology until we understand water* [10]."

A necessary approach to gain deep insights into water is to investigate medium-sized water clusters and their hydrogen bond networks. Water nanoclusters are crucial building blocks of bulk model systems for explaining the anomalous properties of water [11, 12]. However, only indirect experimental information, such as the infrared spectra (IR) [13–32] and photoelectron spectra [33–41], is available for size-nonspecific water clusters. Accordingly, great efforts were devoted to simulating IR spectra in order to assist experiments [42–45].

Until now, several structural motifs of water clusters, such as the fused cage [46, 47], clathrate-like [48, 49], and tubular structures [50], have been proposed. Meanwhile, several optimization approaches combined with empirical potentials were employed to search the most stable structures of different sized water clusters. For example, Hartke systematically examined the structural evolution as a function of size in the regime of $n = 2–30$ with the TIP4P and TTM2-F potentials [51–53]; Thakkar and Kazachenko [54] investigated the global minima of TIP4P water clusters ($n = 6–27$) by basin-hopping algorithm; Liu et al.

Dedicated to Professor Eluvathingal Jemmis and published as part of the special collection of articles celebrating his 60th birthday.

F. Li · Y. Liu · L. Wang · J. Zhao (✉)
School of Physics and Optoelectronic Technology and College of Advanced Science and Technology, Dalian University of Technology, Dalian 116024, China
e-mail: zhaojj@dlut.edu.cn

F. Li
Department of Physics, University of Puerto Rico, San Juan, PR 00931, USA

Z. Chen (✉)
Department of Chemistry, Institute for Functional Nanomaterials, University of Puerto Rico, San Juan, PR 00923, USA
e-mail: zhongfangchen@gmail.com

explored $(H_2O)_{2–34}$ using flexible-body and charge-fluctuating ABEEM/MM water potential model [55]; Yang et al. [56] studied the low-lying structures of $(H_2O)_{20–30}$ based on a combination of the AMOEBA potential and generalized energy-based fragmentation approach; Kazimirski and Buch [57] used the classical TIP4P model and performed MD simulations and rigid-body diffusion Monte Carlo (MC) optimization for water clusters of selected large sizes ($n = 20–22$, 48, 123, and 293).

In spite of those efforts, many fundamental properties of water clusters remain puzzling. It is highly desirable to explore the morphology of water clusters at some reliable and economic level. Following our recent benchmark calculations for small water clusters $(H_2O)_{1–10}$ [58], we continue to examine the energetically favorable structures of water nanoclusters $(H_2O)_n$, $n = 30–48$. The size-dependent evolution of structures and H-bonds, electronic, and vibrational properties will be discussed.

2 Computational methods

In cluster research, it is known that the number of local minima grows rapidly with increasing cluster size. The availability of a myriad of metastable isomers on the potential energy surface (PES) of large water clusters makes the global minimum search a computationally demanding job. This is extremely difficult, if not impossible, to survey such complicated PES using theoretical levels of high accuracy. A wise strategy is to first thoroughly screen the PES using some efficient potentials, then performs computations at more accurate theoretical levels. Here, the energetically favorable structures of $(H_2O)_n$ ($n = 30$, 33, 36, 39, 42, 45, 48) were determined by a combination of MC search and density functional theory (DFT) computations. First, at each cluster size, about six hundreds of isomers were generated randomly and independently using the Metropolis MC algorithm [59] incorporated with TIP4P [60] and TIP5P [61] empirical potentials. During every MC simulations, the lowest energy structures were selected from 7×10^7 MC steps. Then, top six low-energy configurations for the two potentials apiece at each size were further optimized at the DFT level of theory. For comparison, some low-energy isomers from earlier theoretical investigations [45, 51–53, 55–57, 62–67] were also studied in a consistent manner.

According to our benchmark work for small water clusters $(H_2O)_{1–10}$ [58], BLYP [68] is reasonable for describing both the structural and energetic properties of water clusters, and the triple numerical basis set plus polarization functions (TNP) implemented in the DMol^3 program [69, 70] gives satisfactory performance to water clusters. Thus, here we used the high-efficient combination of BLYP and TNP as a practical choice for studying larger sized $(H_2O)_{30–48}$ clusters.

All DFT computations were carried out with the DMol^3 program [69, 70]. Self-consistent field computations were conducted with a convergence criterion of 10^{-6} a.u. on the total energy. All structures were optimized with convergence criteria of 10^{-6} a.u. on the maximum force and 0.005 Å on the maximum displacement of each atom. The real-space global orbital cutoff radius was chosen to be 6.0 Å. All the optimized geometries were characterized as the true local minima by harmonic vibrational frequency analysis.

To further assess the performance of the computational scheme, in Table 1, we compare the computed geometry parameters and physical properties of water monomer and dimer with available experimental data. BLYP/TNP scheme can reasonably reproduce the geometry parameters, electronic properties including dipole moment (μ) and vertical ionization potential (VIP), and vibrational frequencies from experiments.

Table 1 Computed geometry parameters and physical properties for water monomer and dimer compared with available experimental data

Monomer					
	$R_{O–H}$ (Å)	$\theta_{H–O–H}$ (°)	μ (Debye)	VIP (eV)	Frequency (cm^{-1})
BLYP/TNP	0.97	104.3	1.80	12.52	1,606, 3,670, 3,771
Expt.	0.96 [71]	103.9 [71]	1.86 [72]	12.65 [71]	1,595, 3,657, 3,756 [71]

Dimer						
	R_{O-O} (Å)	Strength of hydrogen bond (kcal/mol)	μ (Debye)	VIP (eV)	Frequency (cm^{-1})	
					Free O–H stretching	Hydrogen-bonded O…H
BLYP/TNP	2.94	5.2	2.54	10.79	3,739	3,638
Expt.	2.98 [73]	5.0 ± 0.7 [73]	2.60 [73]	11.21 [71]	3,730 [74]	3,601

Here, VIP is defined as the energy difference between cationic and neutral clusters when both are at the optimized geometry of the neutral cluster

3 Results and discussion

3.1 Structures and stability

Our computations reveal that the most energetically favorable $(H_2O)_{30–48}$ clusters adopt rather complicated configurations with irregular hydrogen bond network, i.e., amorphous core–shell structures (see Fig. 1), which usually exhibit better stability (4.0 ~ 5.5 kcal/mol lower in energy) than the structures reported before, [44, 51–53, 55–58, 60–67] except that $(H_2O)_{48}$ is slightly higher in energy than Qian et al.'s [55] lowest $(H_2O)_{48}$ structure by 0.61 kcal/mol. The improved stability of these newly searched $(H_2O)_{30–48}$ structures is a comprehensive consequence of the number of hydrogen bonds and the strength of hydrogen bonds, which will be discussed in Sect. 3.3.

Here, we cannot guarantee that the present lowest energy configurations are the true global minima, since the potential energy surfaces of these medium-sized clusters are rather complicated. However, the general trend about energetic preference of amorphous core–shell structures in these water clusters would still be valid.

The mean adjacent O–O distances ($R_{O–O}$) for the lowest energy structures reflect the overall structural information of a water cluster, as pointed out in our previous study on $(H_2O)_{2–10}$ clusters. For these most favorable structures of $(H_2O)_n$ (n = 30–48), the average $R_{O–O}$ ranges from 2.80 to 2.81 Å, which seems to be insensitive to cluster size and is very close to the average O–O distance of liquid water (2.82 Å) [75].

Hydrogen bond network plays a major role in the physical and chemical properties of water. For instance, the maximum density of water occurs at 4 °C [76], as a result of competition between the directionality of hydrogen bonding (which favors a lower density) and nondirectional hydrogen bonds, i.e., disorder of water molecules arrangement (which favors a larger density). The influence of the H-bond topology on the stability of water clusters has been the subject of previous studies [77–84].

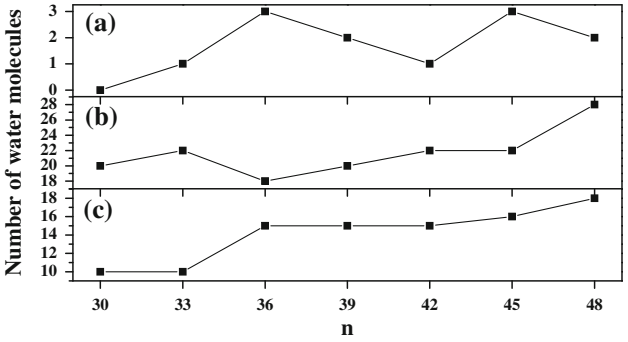

Fig. 2 Number of water molecules with **a** two-coordinated H-bonds, **b** three-coordinated H-bonds, **c** four-coordinated H-bonds

To understand the relative stabilities between isomers, we thus compared the H-bond topological structures of the low-energy configurations for the $(H_2O)_{30–48}$ clusters by counting the number of H-bonds (Fig. 2). As expected, the total number of hydrogen bonds increases as the cluster size increases, while the average number of H-bonds per H_2O molecule remains about 3.3 for all sized clusters explored. There are ~10% interior molecules for these core–shell $(H_2O)_{30–48}$ clusters. All of these clusters are mainly composed of three-coordinated water units and also have significant number (10–18) four-coordinated water (which increases with increasing the cluster size); however, they only have very few (0–3) 1–3 two-coordinated water units, which are all at the irregular shell surface. Note that the three- and four-coordinate water units also dominate in the other regions of phase diagram, such as the crystalline ice forms [85].

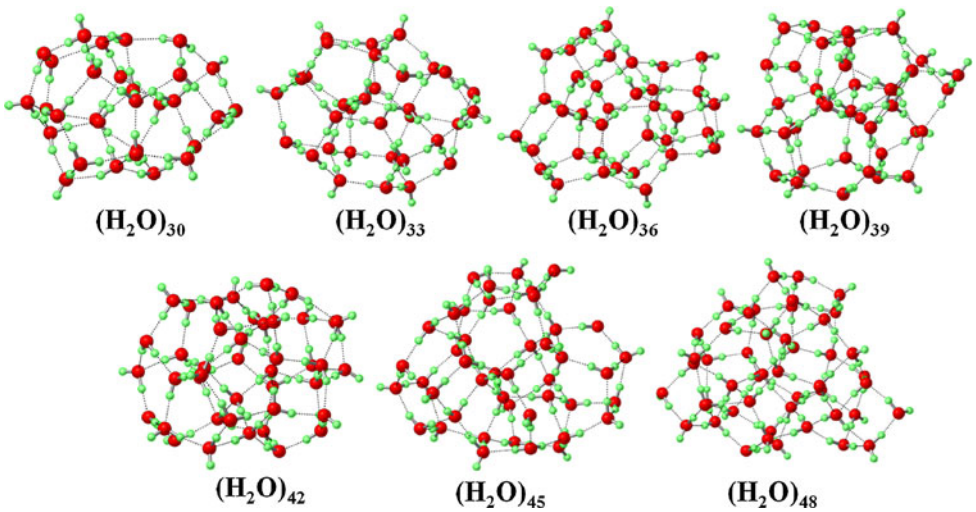

Fig. 1 Lowest energy structures of $(H_2O)_n$ (n = 30–48) clusters

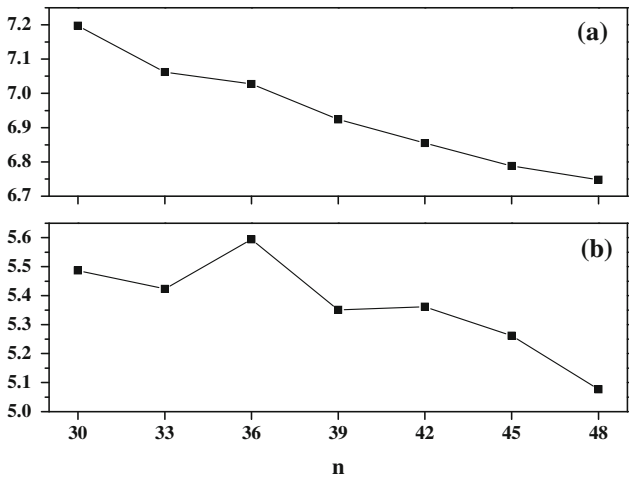

Fig. 3 Electronic properties $(H_2O)_{33–48}$ clusters: **a** VIP and **b** HOMO–LUMO gap. All the values are in eV

Silicon shares the fourfold coordination environment in solid/amorphous phase with water in the liquid/ice states. This reminisces us about the $Si_{27–50}$ clusters [86, 87], which also possess an amorphous structural pattern similar to $(H_2O)_{33–48}$ clusters. Moreover, there are two (three) atoms/molecules in the "core" part of the disordered core–shell structures for both Si_{30} (Si_{33}) and $(H_2O)_{30}$ ($(H_2O)_{33}$), and the number of interior water molecules (1–5) for the $(H_2O)_n$ is similar to the number of Si atoms (1–7) stuffed inside the Si_n clusters for a size range of $n = 30–48$ [86, 87].

3.2 Electronic properties

The size dependence of VIP (vertical ionization potential) is one of the interesting quantities for understanding transitions from molecule to bulk phase. It is also useful to identify a specific cluster by the difference of VIP values in experiments. As listed in Table 1, our computed VIP values for water monomer and dimer (12.52 and 10.79 eV, respectively) agree well with the experimental data (12.65 and 11.21 eV [71], respectively) and the high-level CCSD(T)/aug-cc-pVTZ values (12.67 and 11.81 eV, [88] respectively). According to our computations, the VIP for $(H_2O)_{33–48}$ decreases from 7.20 to 6.75 eV as the cluster size increases (see Fig. 3a).

All these water clusters under study have considerable HOMO (the highest occupied molecular orbital)–LUMO (the lowest unoccupied molecular orbital) gap energies. The HOMO–LUMO gaps oscillate in the range of 5.1 to 5.6 eV (Fig. 3b) and are not sensitive to the size of water clusters for the size range we considered. The sizable HOMO–LUMO gaps can be related to the high kinetic stability of these water clusters.

3.3 Comparisons of three different structural patterns: stabilization energies and IR spectra

In this section, we compare the thermodynamic stabilities and infrared spectra of the amorphous $(H_2O)_{30–48}$ structures with two previous proposed structural motifs, i.e., fused cage [46, 47] and tubular configurations formed by six-membered rings (6MRs) [50].

Stabilization energy (SE) is a key indicator that evaluates the strength of the intermolecular hydrogen bonds in a water cluster. The stabilization energy per molecule for the $(H_2O)_n$ cluster containing n water molecules is defined as $SE = -(E_n - nE_1)/n$, where E_n and E_1 are the total energies of $(H_2O)_n$ cluster and water monomer, respectively. By definition, a larger positive SE value suggests the higher stability of a cluster.

The size-dependent SEs for these three patterns are compared in Fig. 4. Within the size range studied, amorphous structures prevail over the other two motifs. As mentioned before, the stability of water clusters is related with the number of hydrogen bonds and the strength of H-bond, whereas the O…H distance can serve as the index for the strength of hydrogen bonds. Thus, we analyzed the number of hydrogen bonds and the average of O…H distances for the water clusters of the three structural motifs (Table 2). The number of hydrogen bonds of amorphous water clusters is larger than the fused-cage isomers, while the hydrogen bonds are of comparable strength, leading to the larger stabilization energies of amorphous $(H_2O)_{30–48}$. On the other hand, the tubular structures (6MR) have more H-bonds than the amorphous configurations, but the strength of hydrogen bonding is greater in the amorphous clusters, as indicated by the shorter mean O…H distance (by $\sim$0.02 Å). Consequently, the amorphous isomers also possess larger stabilization energies than the tubular forms.

IR spectrum is extremely sensitive to geometric structure and electronic properties, and serves as a useful tool to characterize the structural and bonding behavior of water systems [89–91]. Numerous experimental and theoretical efforts have been devoted to crystalline ice [92], liquid water [93, 94], and water clusters [95–100]. A detailed analysis of the vibrational frequencies in the water clusters enables us to understand the H-bonds and to predict the structural pattern.

In this respect, we compared the IR of three different structural patterns for $(H_2O)_{42}$ cluster as a representative (see Fig. 5). For the H–O–H bending mode (around 1,600 cm^{-1}), the amorphous structure endows more vibration peaks with regard to the other two forms. The O–H stretching mode is sensitive to the strength and coordination of the H-bonds. The intramolecular H-bonds significantly affect the O–H stretching vibrations, and different arrangements between adjacent water units lead to

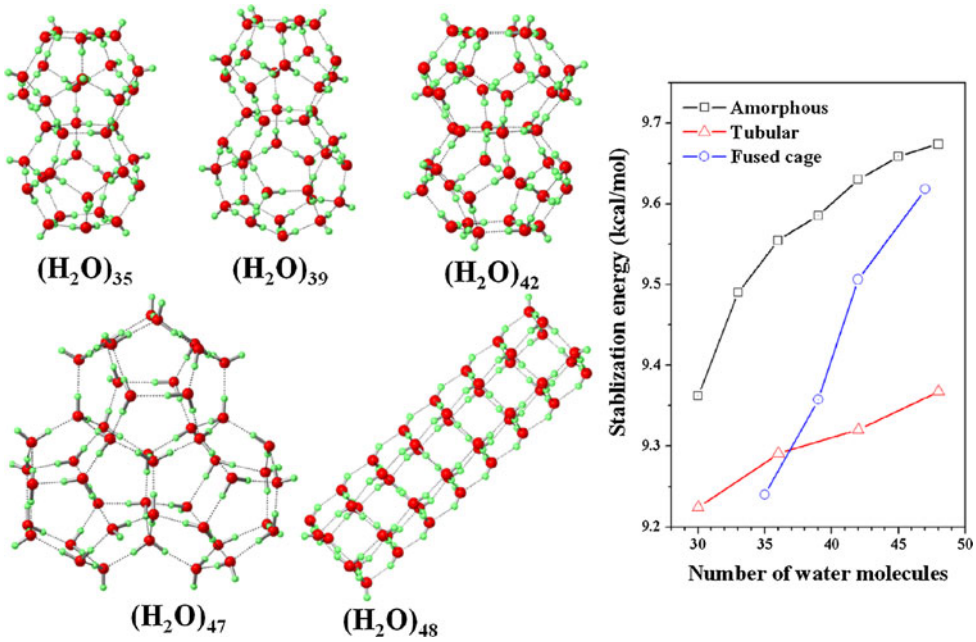

Fig. 4 *Left* fused-cage structures and tubular (6MR) configuration of $(H_2O)_{48}$ (color scheme: O, *red*; H, *green*). *Right* stabilization energies of different structural motifs

Table 2 The number of H-bonds and average of O…H distances (in Å) for the three structural motifs at each size

	Number of H-bonds			Average of O…H distance (Å)		
	Amorphous	Fused cage	6MR	Amorphous	Fused cage	6MR
$n = 30$	50	45	54	1.819	–	1.840
$n = 33$	54	–	–	1.814	–	–
$n = 36$	60	54	66	1.822	1.810	1.831
$n = 39$	65	61	–	1.820	1.805	–
$n = 42$	70	66	78	1.812	1.807	1.839
$n = 45$	74	–	–	1.808	–	–
$n = 47$	–	75	–	–	1.808	–
$n = 48$	80	–	90	1.822	–	1.843

redshift of the corresponding O–H stretch frequencies from that in the gas-phase monomer. For example, Goss et al. [101] experimentally assigned the 3,335 cm^{-1} peak to the bound OH stretching in water clusters in the size of $n = 20$–100, which is redshifted from the symmetric (3,657 cm^{-1}) and anti-symmetric (3,756 cm^{-1}) O–H stretching mode of water monomer by ~320 and 420 cm^{-1}, respectively. For the three structures we considered, it is redshifted up to ~1,000 cm^{-1} from the positions of the symmetric and asymmetric OH stretch vibrations of the free water molecule at 3,657 and 3,756 cm^{-1}, respectively [13], depending on the arrangement of neighboring water molecules. There are seven dominant peaks among the O–H stretching region for the 6MR structure. Compared to the "concise" O–H vibrational frequencies of 6MR-tube, the corresponding stretching modes of the fused-cage and amorphous structures present wider distribution with many vibrational peaks.

These $(H_2O)_{42}$ clusters with different structural patterns have different IR distributions for O–H stretchings. The fused cage has the broadest O–H stretching range, followed by the amorphous and the 6MR structures. The IR distributions of amorphous structure can be traced back to the disordered arrangement of O atoms [102], similar to the inter- and intra-molecular coupling between OH bonds in the proton-disordered crystal [103]. The broadest O–H stretching range in the fused cage can be attributed by the more drastic redshifts of the O–H stretchings in the fused cage due to the disorder of O–H directions. Uniformly, there are peaks around 3,700 cm^{-1} in the simulated IR of all the three structures, which can be assigned to be the free OH stretching modes, as found in the experimental measurements for large clusters (with up to several hundred water molecules) [14–16, 19, 22]. For reference, the IR spectrum of liquid water exhibiting a broad, unstructured distribution with a maximum at 3,400 cm^{-1} [104, 105], whereas the spectrum

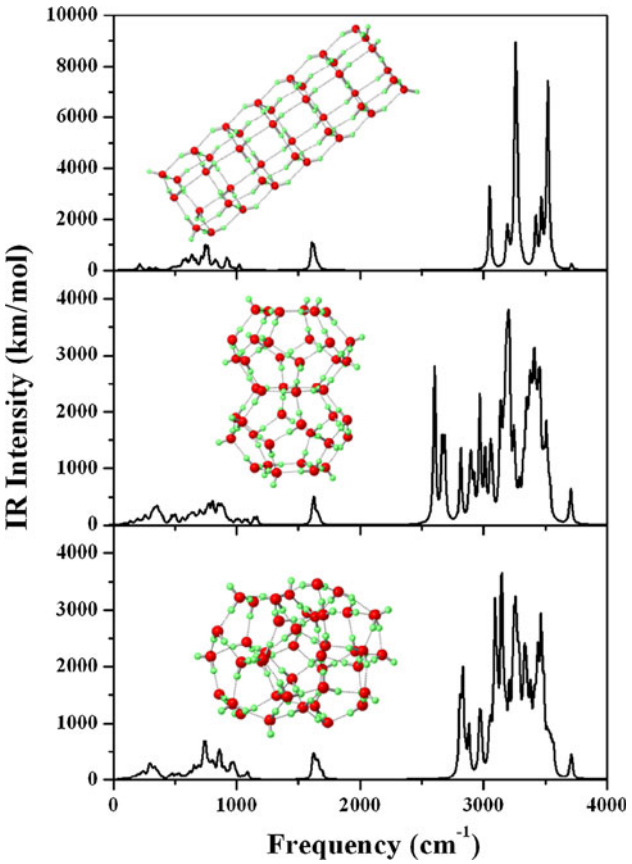

Fig. 5 Comparison of IR spectra for three different structural patterns of $(H_2O)_{42}$ cluster: tubular (*upper*), fused cage (*middle*), amorphous (*lower*)

of amorphous ice shows a similar distribution of peaks around 3,270 cm^{-1} [106].

Despite the computed frequencies are generally larger than the experimental values (such differences can be reduced slightly by a scaling factor), the trends of shifting for the corresponding vibrational modes are expected to be valid and provide useful information for the structural patterns of the medium-sized water clusters.

4 Conclusions

By means of a combination of empirical MC search and density functional theory computations, we obtained the most stable configurations of $(H_2O)_n$ (n = 30–48) clusters with lower energies than earlier reports. Water clusters in such a size range (n = 30–48) energetically prefer amorphous core–shell structures, rather than the symmetric fused cages or tubular configurations with directionality of H-bonds. IR analysis can provide the structural information for experimentalists to further confirm our prediction. The large number and the considerable strength of H-bonds, and the sizable HOMO–LUMO gap contribute to the high stability of the amorphous water clusters. Due to the extreme complicated nature of the potential energy surface, we still cannot guarantee that we have obtained the global minima. Nevertheless, the general trends found for the structural growth pattern of medium-sized clusters should be more or less valid. Our results may provide instructive indications for the evolution toward bulk water from medium-sized clusters.

Acknowledgments This work was supported in China by the National Natural Science Foundation of China (No. 40874039, No. 11174045) and in USA by the NSF Grant (EPS-1010094). We also thank TeraGrid resources for providing CPU time.

References

1. Finney JL (2004) Pjil Trans R Soc Lond B 359:1145–1165
2. Poole PH, Sciortino F, Essmann U, Stanley HE (1992) Nature 360:324–328
3. Ito K, Moynihan CT, Angell CA (1999) Nature 398:492–494
4. Mallamace F, Broccio M, Corsaro C, Faraone A, Majolino D, Venuti V, Liu L, Mou CY, Chen S (2007) Proc Natl Acad Sci 104:424–428
5. Gong X, Li J, Lu H, Wan R, Li J, Hu J, Fang H (2007) Nat Nanotechnol 2:709–712
6. Li J, Gong X, Lu H, Li D, Fang H, Zhou R (2007) Proc Natl Acad Sci 104:3687–3692
7. Gong X, Li J, Zhang H, Wan R, Lu H, Wang S, Fang H (2008) Phys Rev Lett 101:257801–257804
8. Tu Y, Xiu P, Wan R, Hu J, Zhou R, Fang H (2009) Proc Natl Acad Sci 106:18120–18124
9. Rao F, Garrett-Roe S, Hamm PJ (2010) Phys Chem B 114:15598–15604
10. http://news.sciencemag.org/sciencenow/2010/10/at-the-smallest-scale-water-is-a.html
11. Chaplin MF (2000) Biophys Chem 83:211–221
12. Ludwig R (2001) Angew Chem Int Ed 40:1808–1827
13. Dyke TR, Mack KM, Muetner JS (1977) J Chem Phys 66:498–510
14. Vernon MF, Krajnovich DJ, Kwok HS, Lisy JM, Shen YR, Lee YT (1982) J Chem Phys 77:47–57
15. Coker DF, Miller RE, Watts RO (1985) J Chem Phys 82:3554–3562
16. Huang ZS, Miller RE (1989) J Chem Phys 91:6613–6631
17. Buck U, Huisken F (2000) Chem Rev 100:3863–3890
18. Page RH, Vernon MF, Shen YR, Lee YT (1987) Chem Phys Lett 141:1–6
19. Huisken F, Kaloudis M, Kulcke A (1996) J Chem Phys 104:17–25
20. Gruenloh CJ, Carney JR, Arrington CA, Zwier TS, Fredricks SY, Jordan KD (1997) Science 276:1678–1681
21. Paul JB, Collier CP, Saykally RJ, Scherrer JJ, O'Keefe A (1997) J Phys Chem 101:5211–5214
22. Buck U, Ettischer I, Melzer M, Buch V, Sadlej J (1998) Phys Rev Lett 80:2578–2581
23. Brudermann J, Melzer M, Buck U, Kazimirski J, Sadlej J, Buch V (1999) J Chem Phys 110:10649–10652
24. Goss LM, Sharpe SW, Blake TA, Vaida V, Brault JW (1999) J Phys Chem A 103:8620–8624
25. Sadlej J, Buch V, Kazimirski J, Buck U (1999) J Phys Chem A 103:4933–4947
26. Goss LM, Sharpe SW, Blake TA, Vaida V, Brault JW (1999) J Phys Chem A 103:8620–8624

27. Devlin JP, Sadlej J (2001) Buch. J Phys Chem A 105:974–983
28. Anderssona P, Steinbach C, Buck U (2003) Eur Phys J D 24:53–56
29. Shin JW, Hammer NI, Diken EG, Johnson MA, Walters RS, Jaeger TD, Duncan MA, Christie RA, Jordan KD (2004) Science 304:1137–1140
30. Steinbach C, Andersson P, Kazimirski JK, Buck U, Buch V, Beu TA (2004) J Phys Chem A 108:6165–6174
31. Roscioli JR, Hammer NI, Johnson MA (2006) J Phys Chem A 110:7517–7520
32. Hamashima T, Mizuse K, Fujii A (2011) J Phys Chem A 115:620–625
33. Coe JV, Lee GH, Eaton JG, Arnold ST, Sarkas HW, Bowen KH, Ludewigt C, Haberland H, Worsnop DR (1990) J Chem Phys 92:3980–3982
34. Campagnola PJ, Lavrich DJ, DeLuca MJ, Johnson MA (1991) J Chem Phys 94:5240–5242
35. Ayotte P, Johnson MA (1997) J Chem Phys 106:811–814
36. Kim J, Becker I, Cheshnovsky O, Johnson MA (1998) Chem Phys Lett 297:90–96
37. Bragg AE, Verlet JRR, Kammrath A, Cheshnovsky O, Neumark DM (2004) Science 306:669–671
38. Bragg AE, Verlet JRR, Kammrath A, Cheshnovsky O, Neumark DM (2005) J Am Chem Soc 127:15283–15295
39. Kammrath A, Verlet JRR, Griffin GB, Neumark DM (2006) J Chem Phys 125:076101–076102
40. Ma L, Majer K, Chirot F, Issendorff BV (2009) J Chem Phys 131:144303–144306
41. Griffin GB, Young RM, Ehrler OT, Neumark DM (2009) J Chem Phys 131:194302–194309
42. Lenz A, Ojamäe L (2006) Chem Phys Lett 41:8361–8367
43. Fanourgakis GS, Aprà E, Jong WA, Xantheas SS (2005) J Chem Phys 122:134304–134309
44. Lagutschenkov A, Fanourgakis GS, Niedner-Schatteburg G, Xantheasa SS (2005) J Chem Phys 122:194310–194319
45. Mizuse K, Hamashima T, Fujii A (2009) J Phys Chem A 113:12134–12141
46. Khan A (1997) J Chem Phys 106:5537–5540
47. Khan A (1999) J Phys Chem A 103:1260–1264
48. Chaplin MF (1999) Biophys Chem 83:211–221
49. Ludwig R, Appelhagen A (2005) Angew Chem Int Ed 44:811–815
50. Bai J, Su CR, Parra RD, Zeng XC, Tanaka H, Koga K, Li JM (2003) J Chem Phys 118:3913–3916
51. Hartke B (2003) Phys Chem Chem Phys 5:275–284
52. Hartke B (2003) Eur Phys J D 24:57–60
53. Hartke B (2002) Angew Chem Int Ed 41:1468–1487
54. Kazachenko S, Thakkar A (2009) J Chem Phys Lett 476:120–124
55. Qian P, Lu L, Song W, Yang Z (2009) Theor Chem Acc 123:487–500
56. Yang Z, Hua S, Hua W, Li S (2010) J Phys Chem A 114:9253–9261
57. Kazimirski JK, Buch V (2003) J Phys Chem A 107:9762–9775
58. Li F, Wang L, Zhao JJ, Xie RH, Riley K, Chen Z (2011) Theor Chem Acc 131:1163–1169
59. Metropolis N, Rosenbluth1 AW, Rosenbluth1 MN, Teller1 AH, Teller E (1953) J Chem Phys 21:1087–1092
60. Jorgensen WL, Chandrasekhar J, Madura JD, Impey RW, Klein ML (1983) J Chem Phys 79:926–935
61. Mahoney MW, Jorgensen WL (2000) J Chem Phys 112:8910–8922
62. Nigra P, Kais S (1999) Chem Phys Lett 305:433–438
63. Hartke B (2003) Phys Chem Chem Phys 5:275–284
64. Lenz A, Ojamäe L (2006) J Phys Chem A 110:13388–13393
65. Bandow B, Hartke B (2006) J Phys Chem A 110:5809–5822
66. Takeuchi H (2008) J Chem Inf Model 48:2226–2233
67. Liu X, Lu WC, Wang CZ, Ho KM (2011) Chem Phys Lett 508:270–275
68. Becke AD (1988) Phys Rev A 38:3098–3100
69. Delley B (1990) J Chem Phys 92:508–517
70. Delley B (2000) J Chem Phys 113:7756–7764
71. http://webbook.nist.gov/chemistry/ and references therein
72. Lovas FJ (1978) J Phys Chem Ref Data 7:1445–1750
73. Dyke TR, Mack KM, Muenter JS (1977) J Chem Phys 66:498–510
74. Huisken F, Kaloudis M, Kulcke A (1999) J Chem Phys 104:17–25
75. Narten AH, Levy HA (1969) Science 165:447–454
76. Kotz JC, Treichel P, Weaver GC (2005) Chemistry & Chemical Reactivity. Thomson Brooks/Cole, ISBN 053439597X
77. McDonald S, Ojamäe L, Singer SJ (1998) J Phys Chem A 102:2824–2832
78. Kuo JL, Ciobanu CV, Ojamäe L, Shavitt I, Singer SJ (2003) J Chem Phys 118:3583–3588
79. Belair SD, Francisco JS (2003) Phys Rev A 67:063206–063207
80. Tissander MD, Singer SJ, Coe JV (2000) J Phys Chem A 104:752–757
81. Anick DJ (2002) J Mol Struct (THEOCHEM) 587:87–96
82. Anick DJ (2003) J Chem Phys 119:12442–12456
83. Chihaia V, Adams S, Kuhs WF (2004) Chem Phys Lett 297:271–287
84. Kirov MV (2002) J Struct Chem 5:790–797
85. Ludwig R, Weinhold F (1999) J Chem Phys 110:508–515
86. Yoo S, Zhao J, Wang J, Zeng XC (2004) J Am Chem Soc 126:13845–13849
87. Zhao J, Wang J, Jellinek J, Yoo S, Zeng XC (2005) Eur Phys J D 34:35–37
88. Ferreira C, Martiniano HFMC, Cabral BJC, Aquilanti V (2010) Int J Quant Chem 111:1824–1835
89. Huang ZS, Miller RE (1989) J Chem Phys 91:6613–6631
90. Paul JB, Provencal RA, Chapo C, Roth K, Casaes R, Saykally RJ (1999) J Phys Chem A 103:2972–2974
91. Steinbach C, Andersson P, Kazimirski JK, Buck U, Buch V, Beu TA (2004) J Phys Chem A 108:6165–6174
92. Devlin JP, Sadlej J, Buch V (2001) J Phys Chem A 105:974–983
93. Buch V (2005) J Phys Chem B 109:17771–17774
94. Schmidt DA, Miki K (2007) J Phys Chem A 111:10119–10122
95. Steinbach C, Andersson P, Kazimirski JK, Buck U, Buch V, Beu TA (2004) J Phys Chem A 108:6165–6174
96. Buck U, Huisken F (2000) Chem Rev 100:3863–3890
97. Ohno K, Okimura M, Akai N, Katsumoto Y (2005) Phys Chem Chem Phys 7:3005–3014
98. Dunn ME, Evans TM, Kirschner KN, Shields GC (2006) J Phys Chem A 110:303–309
99. Lenz A, Ojamäe L (2006) J Phys Chem A 110:13388–13393
100. Anick DJ (2006) J Phys Chem A 110:5135–5143
101. Goss LM, Sharpe SW, Blake TA, Vaida V, Brault JW (1999) J Phys Chem A 103:8620–8624
102. Baragiola RA (2003) In water in confining geometries. Buch V, Devlin JP, (eds) Springer, Berlin, p 359
103. Buch V, Devlin JP (1999) J Chem Phys 110:3437–3443
104. Bertie JE, Lan Z (1996) Appl Spectrosc 50:1047–1057
105. Walrafen GE (1967) J Chem Phys 47:114–126
106. Bergren MS, Schuh D, Sceats MG, Rice SA (1978) J Chem Phys 69:3477–3482